Physics and Chemistry of Minerals (2019) 46:807–814
https://doi.org/10.1007/s00269-019-01041-1

ORIGINAL PAPER

The pressure-induced phase transition(s) of $ZrSiO_4$: revised

Experimental proof for the existence of a new high-pressure polymorph of zircon

Boriana Mihailova[1] · Naemi Waeselmann[1] · Claudia Stangarone[2] · Ross J. Angel[3] · Mauro Prencipe[4] · Matteo Alvaro[3]

Received: 1 April 2019 / Accepted: 29 May 2019 / Published online: 22 June 2019

Abstract
The existence of a new high-pressure low-symmetry (HPLS) $ZrSiO_4$ phase (space group $I\bar{4}2d$), which has been predicted by density-functional-theory (DFT) calculations (Stangarone et al. in Am Mineral, 2019b), is experimentally confirmed by in situ high-pressure Raman spectroscopic analysis up to 25.3 GPa. The new $ZrSiO_4$ polymorph is developed from zircon via a soft-mode-driven displacive phase transition. The Cochran-law-type pressure dependency of the soft-mode wavenumber reveals a zircon-to-HPLS critical pressure $p_c = 20.98 \pm 0.02$ GPa. The increase in the phonon compressibilities of the zircon hard mode near 202 cm^{-1} at $p > p_r = 10.0$ GPa as well as of the reidite hard mode near 349 cm^{-1} at $p < p_r$ marks the pressure above which zircon becomes thermodynamically metastable with respect to reidite; the experimentally determined value of p_r is in good accordance with the equilibrium zircon–reidite transition pressure derived from DFT simulations. However, at room temperature, there is not enough driving force to rebuild the atomic linkages and the reconstructive transition to reidite happens ~ 1.4 GPa above p_c, indicating that at room temperature, the HPLS phase is a structural bridge between zircon and reidite. The pressure dependencies of the phonon modes in the range 350–460 cm^{-1} reveal that the reconstructive phase transition in the $ZrSiO_4$ system is triggered by energy resonance and admixture of hard modes from the parent and resultant phase.

Keywords Zircon · High pressure · Phase transition · Raman spectroscopy · Soft mode

Introduction

Zircon ($ZrSiO_4$, space group $I4_1/amd$) is a widespread accessory mineral, extensively used to follow the paragenesis and evolution of rocks, because its atomic structure is stable over a wide temperature and pressure range, and thus, crystals of zircon can survive several stages of the geological rock cycling. Moreover, due to the thermo-mechanical strength and chemical inertness of zircon as well as its structural resistivity to radiation damage, zircon-based ceramics are promising technological materials with applications as refractory ceramics as well as for encapsulation of radioactive waste products. Because of its importance in Earth and materials sciences, zircon has been comprehensively studied under non-ambient conditions. At low pressures, the temperature stability field of zircon extends to the melting point (≥ 2200 K). Reidite is the known high-pressure (HP) polymorph of $ZrSiO_4$, which has a scheelite-type structure (space group $I4_1/a$) and occurs associated with shock-metamorphized zircon (Montalvo et al. 2019). Experimentally, the phase boundary between zircon and reidite has been established to be around 9 GPa in the temperature range 1200–1900 K (Ono et al. 2004). Based on HP studies using the diamond-anvil cell (DAC) method, it has been suggested that at room temperature, the pressure-induced

Electronic supplementary material The online version of this article (https://doi.org/10.1007/s00269-019-01041-1) contains supplementary material, which is available to authorized users.

✉ Boriana Mihailova
boriana.mihailova@uni-hamburg.de

[1] Department of Earth Sciences, University of Hamburg, 20146 Hamburg, Germany

[2] Institute for Planetary Research, German Aerospace Centre (DLR), Rutherfordstr. 2, 12489 Berlin, Germany

[3] Department of Earth and Environmental Sciences, University of Pavia, Via A. Ferrata 1, 27100 Pavia, Italy

[4] Earth Sciences Department, University of Torino, Via Valperga Caluso 35, Turin, Italy

phase transition from zircon to reidite occurs near 20–23 GPa (Knittle and Williams 1993; van Westrenen et al. 2004). Although the space group of reidite appears to be a subgroup of that of zircon, the zircon-to-reidite transition is reconstructive, involving alteration of the bond topology (Stangarone et al. 2019b).

Recent high-pressure Raman scattering analyses of well-crystalline and radiation-damaged zircon have revealed a gradual softening of the lowest energy Raman-active phonon mode ($E_g \sim 202\ cm^{-1}$) when pressure increases from ambient to 8 GPa, independently of the degree of structural disorder (Pina Binvignat et al. 2018). Soft-mode-driven structural transformations are, however, typical of displacive phase transitions that are thermodynamically of second order, and therefore, the observed softening should not be exclusively related to the zircon–reidite reconstructive transition. To shed light on this puzzling phonon behaviour and to explore more in detail the structure and atomic dynamics at high pressures, density-functional-theory (DFT) calculations of $ZrSiO_4$ have been very recently performed (Stangarone et al. 2019b). The DFT simulations reveal that there should be two pressure-induced phase transitions of $ZrSiO_4$: (i) a reconstructive zircon–reidite phase transition at $p_r \sim 9$–10 GPa, which is associated with thermodynamic instability due to the crossing of the Gibbs energies of zircon and reidite, making zircon metastable above p_r and (ii) a displacive phase transition at $p_c \sim 20$ GPa from zircon to a new high-pressure low-symmetry (HPLS) phase with space-group symmetry $I\bar{4}2d$, which is associated with a lattice-dynamics instability triggered by a soft mode. The soft mode consists of SiO_4 rigid rotations about the *c*-axis, reflecting the structural difference between the two phases (see Fig.1). It is silent in the zircon phase (B_{1u} mode in $I4_1/amd$) and becomes Raman-active above p_c (A_1 mode in $I\bar{4}2d$). Moreover, the DFT simulations reveal that due to the pressure-enhanced lattice-dynamics instability, two Raman-active hard modes of zircon, E_g near 202 cm^{-1} and B_{2g} near 265 cm^{-1}, soften when approaching p_c, most probably because they also involve rotation/twisting of SiO_4 and ZrO_8 polyhedra about the *c*-axis (Stangarone et al. 2019a) and can easily couple with the soft mode. The phonon mode $B_{2g} \sim 265\ cm^{-1}$ is very weak (Kolesov et al. 2001) and difficult to measure in DAC, but the theoretically predicted pressure behaviour of $E_g \sim 202\ cm^{-1}$ is in full accordance with the experimental data up to 10 GPa (Pina Binvignat et al. 2018).

The re-inspection of the previously reported pressure–volume (*p*–*V*) experimental data of $ZrSiO_4$ (van Westrenen et al. 2004) actually reveals that the calculated *V*(*p*) dependence of the HPLS phase better matches the data above 20 GPa as compared to that of zircon (Stangarone et al. 2019b). However, the experimentally observed phase transition near 20–23 GPa has so far been associated with the formation of reidite, coexisting with zircon, most probably because the X-ray diffraction (XRD) pattern as well as the Raman scattering above 150 cm^{-1} resembles that of zircon. According to the DFT calculations, the soft-mode wavenumber is 94 cm^{-1} at 20 GPa (Stangarone et al. 2019b). Neither zircon, nor reidite exhibits Raman-active modes below 150 cm^{-1} (Stangarone et al. 2019b), and therefore, the new HPLS phase can be distinctly detected by the presence of a low-energy Raman peak generated by the A_1 soft mode.

Here, we report the results of our in situ HP Raman scatting experiments up to ~ 25.3 GPa, which unambiguously confirm the occurrence of a soft-mode-driven phase transition at $p_c = 21.0(1)$ GPa and the formation of the new high-pressure $ZrSiO_4$ polymorph. The zircon hard mode at ~ 202 cm^{-1} couples with the soft mode, leading to a

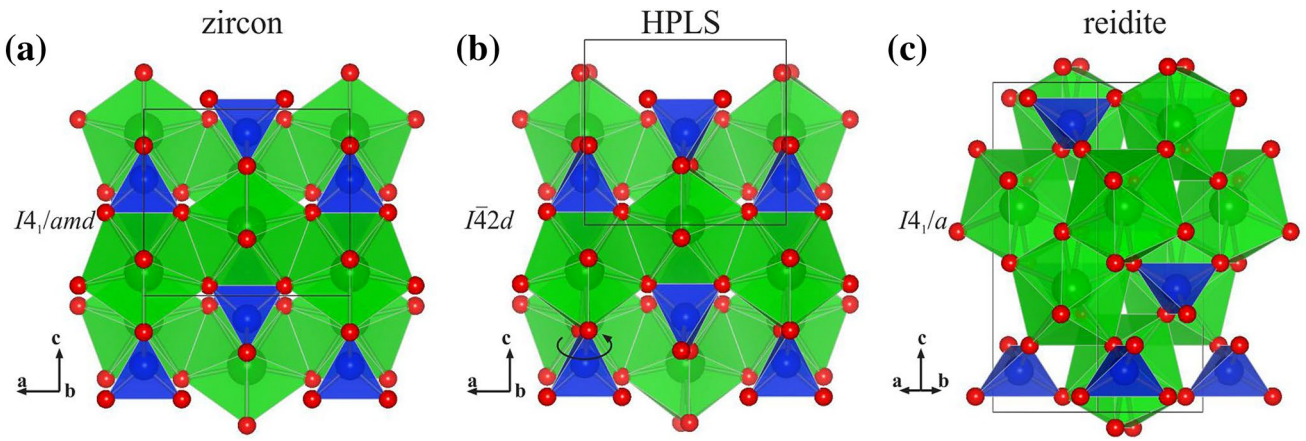

Fig. 1 Comparison of the three $ZrSiO_4$ polymorphs: zircon (**a**), HPLS (**b**), and reidite (**c**); SiO_4 tetrahedra are shown in blue, ZrO_8 polyhedra in green. Structural data of zircon are after Robinson et al. (1971), and the atomic positions for HPLS (at 21 GPa) and reidite (at 0 GPa) are derived from DFT simulations (Stangarone et al. 2019b). The figure was prepared using the VESTA software package (Momma and Izumi 2008)

minimum of the hard-mode wavenumber near p_c. Furthermore, $d\omega/dp$ of this hard mode abruptly changes at 10.0 GPa, near p_r predicted by DFT calculations, indicating perturbations in the shape of the corresponding local potential. However, reidite was only detected above 21.0 GPa, revealing that at room temperature, the activation barrier between zircon and reidite can be overcome via the formation of the HPLS phase as an intermediate bridging state between zircon and reidite.

Experimental details

Samples

Optically homogeneous gem-quality pale-pinkish euhedral natural crystals of size $\sim 1 \times 1 \times 2$ mm^3 were used in this study. The chemical homogeneity was confirmed by backscattered electron imaging and the composition was determined by wavelength-dispersive electron microprobe analysis over 25 points (Cameca SX-100 SEM system). The derived chemical formula is $Zr_{1.0104(28)}Hf_{0.0097(3)}Si_{0.9709(29)}P_{0.0073(3)}O_4$. The zircon sample was also probed for Mg, Al, Ca, Mn, Fe, Y, Ce, Nd, Pb, Th, and U, but their amounts were below the detection limit.

Oriented (100) plates from the same crystal subjected to chemical analysis were cut with a diamond wire saw and polished down to $\sim$ 20 µm. Two specimens sized $\sim 29 \times 44 \times 17$ and $\sim 62 \times 32 \times 26$ µm^3 (referred here after as A1 and A2) were loaded in two Boehler–Almax DACs equipped with diamonds having a culet diameter of 500 and 600 µm, respectfully. Rhenium gaskets with a thickness of 0.2 mm were initially indented to ~60 µm. Holes with a diameter of 300 µm were drilled using an Almax-easyLab spark eroder with tungsten carbide tips. Helium as a pressure transmitting was used, because it shows negligibly small non-hydrostaticity up to 30 GPa (Klotz et al. 2009). The pressure p was determined via the ruby photoluminescence R1 line (Munro et al. 1985) with a precision of $\sim$ 0.1 GPa.

Raman spectroscopy

Raman experiments were done with a Horiba Jobin-Yvon T64000 triple-monochromator system equipped with a Symphony LN_2-cooled CCD detector and an Olympus BH41 microscope with a 50× long-working-distance objective. The Raman scattering was excited with the 514.532-nm line of a Coherent Innova 90C FreD Ar^+ laser. Spectra at ambient pressure were also measured using the 488-nm laser line to discriminate the Raman scattering signals above 1000 cm^{-1} from the photoluminescence peaks, arising from trace elements (Nasdala et al. 2004). The spectral resolution was approximately 2 cm^{-1}, while the instrumental precision in the peak positions was 0.35 cm^{-1}. First, polarized spectra in the range 15–1215 cm^{-1} were collected from sample A2 in $\bar{y}(zz)y$, $\bar{y}(xz)y$, and $\bar{y}(xx)y$ scattering geometries (Porto's notation), where x, y, and z were approximately along the [100], [010], and [001] directions of zircon, respectively. Then, $\bar{y}(zz)y$ and $\bar{y}(xz)y$ spectra from sample A1 were collected with a smaller pressure step near the experimentally detected critical pressure. The $\bar{y}(zz)y$ scattering geometry was preferred over $\bar{y}(xx)y$, because the strongest polarizability-tensor component of the soft mode is α_{zz} (Stangarone et al. 2019b), and due to the displacive nature of the phase transition, the HPLS phase should occur with its **c** axis oriented along the same direction as the **c** axis of the parent zircon phase. When a new spectral feature appeared at a certain pressure, spectra were collected from several other points on the sample to verify the reproducibility of the observed Raman signal. Spectra in the range 1050–1600 cm^{-1} arising from the diamond anvils were also collected, to follow the stress-induced morphic effects on the diamond structure and the consequent depolarization of Raman scattering due to stress-induced changes in the optical properties of the anvils. At each pressure step, a background spectrum was measured aside from the sample and subsequently subtracted from the sample spectrum. The spectra were further temperature-reduced to account for the Bose–Einstein phonon population factor, using the relation $I_{reduced} = I_{measured}/\{[\exp(\hbar\omega/k_B T) - 1]^{-1} + 1\}$, where $\hbar$, ω, k_B, and T are the reduced Planck constant, phonon angular frequency, Boltzmann constant and temperature, respectively. The reduced spectra were fitted with pseudo-Voigt peak-shape functions $PV = qL + (1 - q)G$ (L and G stand for Lorentz and Gauss peak-shape functions, respectively, q is a weight coefficient) to determine the peak positions ω, full-width at half-maximum (FWHMs, Γ), and integrated intensities I.

Results and discussion

Figure 2 shows selected Raman spectra measured in situ at different pressures in $\bar{y}(zz)y$ scattering geometry, where the Raman-active soft mode of the new HPLS phase is expected to be most pronounced (Stangarone et al. 2019b). According to group-theory analysis (see Table 1), at ambient pressure only the A_{1g} modes of zircon are symmetry allowed in the $\bar{y}(zz)y$ spectra (peaks at 439 and 975 cm^{-1}), but the B_{1g} near 215 and 1008 cm^{-1} as well as the E_g near 202, 224, and 357 cm^{-1} are also observed due to imperfect sample orientation. The experimental run on sample A2 showed the presence only of zircon up to 21.0 GPa. A low-energy Raman peak near 66 cm^{-1} was observed for A2 at the next pressure step, at 22.3 GPa. Our DFT calculations have shown that the

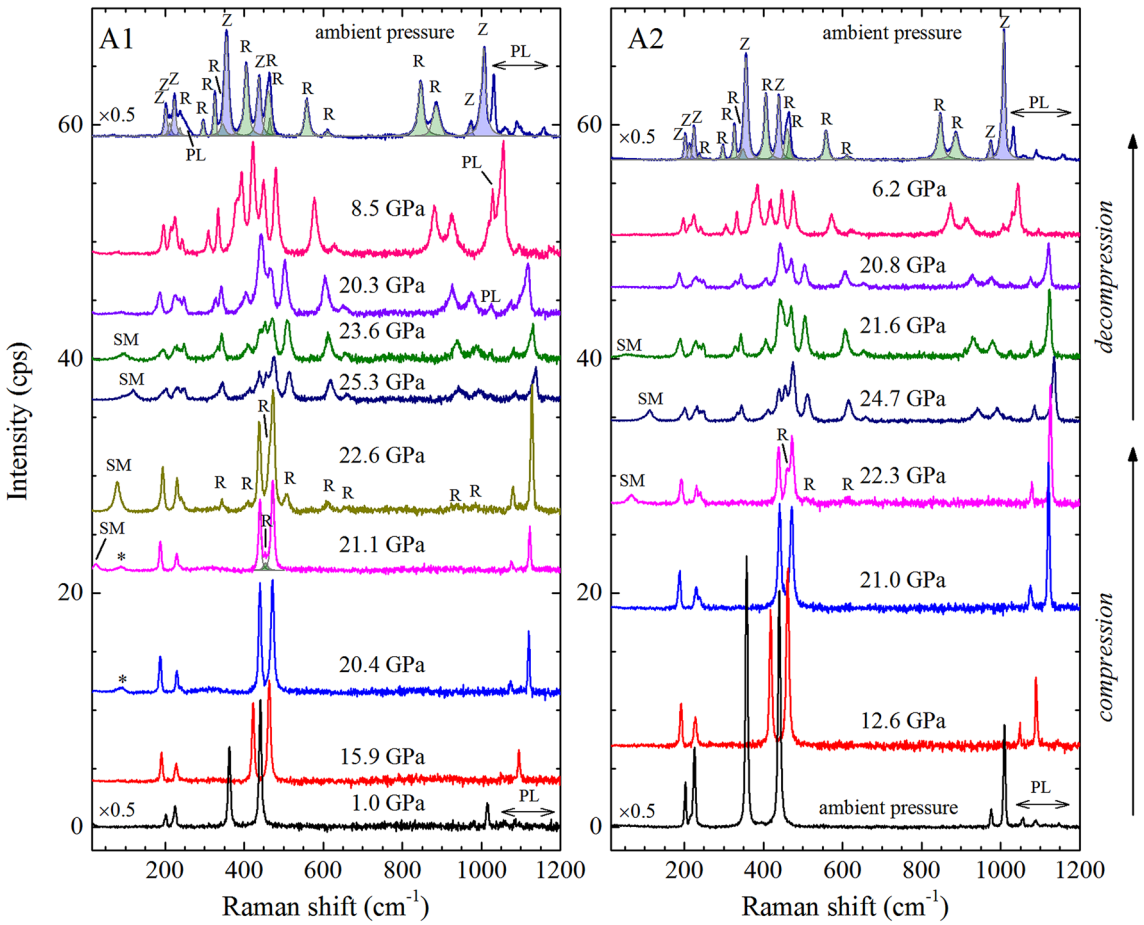

Fig. 2 $\bar{y}(zz)y$ Raman spectra of $ZrSiO_4$ collected at different pressures from sample A1 (left) and A2 (right); SM denotes the Raman-active soft mode in the HPLS phase, the peaks arising from reidite near 22 GPa are marked by R; the zircon and reidite peaks in the ambient-pressure spectra measured after decompression are shaded in blue and green, respectively, and marked by Z and R. The peak at 454 cm^{-1} due to reidite-type intermediate-range order observed at 21.1 GPa for sample A1 is also shaded in green. Photoluminescence peaks are marked by PL. The Raman scattering marked by asterisks in the spectra of A1 at 20.4 and 21.1 GPa is attributed to anomalous Raman activity of the zircon silent B_{1u} soft mode, resulting from incipient disturbance of symmetry at the time scales of phonon lifetimes

only possible origin of such a low-energy peak is the occurrence of Raman activity of the soft mode upon the transformation of the phonon symmetry from B_{1u} to A_1 when the symmetry of the structure changes from $I4_1/amd$ to $I\bar{4}2d$. Thus, this low-energy Raman peak unambiguously reveals the existence of a new HP polymorph of zircon

At this pressure, three additional peaks, near 460, 509, and 610 cm^{-1}, associated with reidite were also resolved. However, the reidite peaks in the range 800–1000 cm^{-1}, arising from SiO_4 stretching modes, were not observed at 22.3 GPa, although at further pressures, they are similar in intensity to the modes near 509 and 610 cm^{-1}. Besides, the sample remained optically homogeneous and transparent, which excludes a reconstructive phase transition involving multiple nucleation of randomly oriented grains of the new phase. Therefore, we attribute the appearance of the peaks 460, 509, and 610 cm^{-1} to incipient reidite-type precursor clusters. The reidite SiO_4-stretching peaks as well as the rest of the reidite peaks were detected ~ 1 GPa higher, at 23.3 GPa, at which pressure the sample became opaque and the spectra depolarized (see the Supplementary Material), indicating the development of reidite long-range order in the form of randomly oriented crystallites coexisting with the HPLS phase. On decompression, the HPLS phase transformed back to zircon, whereas reidite was quenched. The run on sample A1 confirmed these observations. The Raman-active soft mode of the HPLS phase was first detected at 21.1 GPa, with a single extra peak at 454 cm^{-1} that could be related to reidite-type incipient clusters. Reidite long-range order occurred at 22.6 GPa, where most of the reidite peaks were resolved, the Raman scattering depolarized and the sample lost transparency. Thus, by combining the data collected from both samples, one can firmly establish that at room temperature under hydrostatic pressure zircon reversibly

Table 1 Site-symmetry analysis of the phonon modes at the Brillouin-zone centre Γ in zircon, HPLS, and reidite as well as phonon Raman activity in the experimental geometries used in this study. The table was prepared using the online tools of the Bilbao crystallographic server (Kroumova et al. 2003)

	zircon ($I4_1/amd$, SG #141)	HPLS ($I\bar{4}2d$, SG #122)	reidite ($I4_1/a$, SG #88)
Zr	$A_{2u} + B_{1g} + E_g + E_u$	$B_1 + B_2 + 2E$	$A_u + B_g + \{^1E_g + ^2E_g\} + \{^1E_u + ^2E_u\}$
Si	$A_{2u} + B_1g + E_g + E_u$	$B_1 + B_2 + 2E$	$A_u + B_g + \{^1E_g + ^2E_g\} + \{^1E_u + ^2E_u\}$
O	$2A_1g + A_{1u} + A_{2g} + 2A_{2u} + 2B_{1g} + B_{1u} + B_{2g} + 2B_{2u} + 3E_g + 3E_u$	$3A_1 + 3A_2 + 3B_1 + 3B_2 + 6E$	$3A_g + 3A_u + 3B_g + 3B_u + \{^1E_g + ^2E_g\} + \{^1E_u + ^2E_u\}$
$\Gamma_{acoustic}$	$A_{2u} + E_u$	$B_2 + E$	$A_u + \{^1E_u + ^2E_u\}$
$\Gamma^a_{optical}$	$2A_1g(R) + A_{1u}(ina) + A_{2g}(ina) + 3A_{2u}(IR) + 4B_1g(R) + B_{1u}(ina) + B_{2g}(R) + 2B_{2u}(ina) + 5E_g(R) + 4E_u(IR)$	$3A_1(R) + 3A_2(ina) + 5B_1(R) + 4B_2(R, IR) + 9E(R, IR)$	$3A_g(R) + 3A_u(IR) + 3B_g(R) + 3B_u(ina) + \{^1E_g + ^2E_g\}(R) + \{^1E_u + ^2E_u\}(IR)$
Allowed modes			
In $\bar{y}(zz)y$	A_{1g}	A_1	A_g
In $\bar{y}(xz)y$	E_g	E	$\{^1E_g + ^2E_g\}^b$
In $\bar{y}(xx)y$	A_{1g}, B_{1g}	A_1, B_1	A_g

[a] R, Raman-active; IR, infrared-active; ina, inactive;

[b] ^1E_g and ^2E_g are complex conjugates and a pair of them gives rise to a single peak

transforms into a HPLS phase near 21 GPa, while reidite is irreversibly formed between 22.3 and 22.6 GPa.

The pressure dependence of the wavenumber of the HPLS A_1 soft mode follows a Cochran-type law $\omega(p) = c(p - p_c)^n$ (see Fig. 3), and the power-function fit to the data points reveals a critical pressure $p_c = 20.98 \pm 0.02$ GPa and a critical exponential $n = 0.43 \pm 0.02$. An interesting feature is the Raman scattering near 88 cm^{-1} observed for A1 at 20.4 GPa (marked by asterisk in Fig. 2). This peak becomes less pronounced when the HPLS A_1 mode appears at 21.1 GPa and vanishes at higher pressures. On decompression, it reappears just below p_c as a very weak and broad signal and disappears on further decompression. We attribute this Raman scattering to anomalous Raman activity of the zircon B_{1u} soft mode, resulting from incipient removal of point-symmetry elements (e.g., $\bar{1}$) in the vicinity of p_c. The non-zero Raman intensity of this otherwise silent soft mode in zircon is probably triggered by inherent structural defects and intrinsic strain inhomogeneities, the presence of which results also in its non-zero wavenumber near p_c (see Fig. 3) Such anomalous Raman scattering was not observed for sample A2.

Figure 4 shows the pressure dependence of the wavenumber of the zircon E_g phonon mode ~ 202 cm^{-1}, which above p_c transforms into an *E* mode of the HPLS phase. This hard mode clearly softens on the approach to p_c from both sides, in full accordance with the DFT calculations. On compression, $\omega_{202}(p)$ exhibits a plateau-like minimum between 19.5 and 21.0 GPa, indicating ongoing lattice-dynamics instabilities leading to a flattening of the crystal potential and a consequent displacive phase transition. Note that in this pressure range, the zircon soft mode, which was anomalously observed in the Raman spectra, also remains constant in wavenumber (see Fig. 3). Another important feature of the zircon E_g hard mode ~ 202 cm^{-1} is that on compression $d\omega/dp$ changes abruptly at 10.0 GPa (see Fig. 4). The deviation of $\omega_{202}(p)$ from the initial linear trend indicates a change in the interatomic force constants, that is, a change in the shape of local potentials. This is associated with the thermodynamic metastability of zircon above 10.0 GPa, as revealed by DFT calculations (Stangarone et al. 2019b). This conclusion is supported by the fact that below 10 GPa, where reidite is thermodynamically metastable, the wavenumbers of a few low-energy Raman-active modes of reidite deviate from the linear pressure dependence observed in the range 10–25.3 GPa. This deviation is most strongly pronounced for the reidite B_g mode near 349 cm^{-1} (see Fig. 5). Thus, Raman experiments indicate that at room temperature, zircon is metastable above p_r ~10 GPa, which is in a good accordance with the value of equilibrium zircon–reidite transition pressure ~ 9.1 GPa derived from DFT simulations at 0 K. However, room temperature is not sufficient to overcome the potential barrier between zircon and reidite and to rebuild the Si–O–Zr bridges in the pressure range ~ 10–21 GPa. It should be mentioned that a high density of structural defects can influence p_r. For example, zircon with a high degree of radiation-induced structural damage (accumulated radiation dose ~ 6.8×10^{18} α-decay events.g^{-1}) exhibits a kink in $\omega_{202}(p)$ at 8.5 GPa (Pina Binvignat et al. 2018), suggesting that the process of metamictization shifts the stability field of zircon towards lower pressures.

The atomistic mechanism of the reconstructive transition in the $ZrSiO_4$ system can be inferred from the pressure dependence of the Raman-active hard modes in the range 350–460 cm^{-1} (see Fig. 6). Zircon exhibits two strong Raman

Table 2 Hard-mode phonon wavenumbers ω (in cm^{-1}), pressure derivatives $d\omega/dp$ (in $cm^{-1}GPa^{-1}$), and phonon compressibilities $\beta_\omega = \frac{1}{\omega_0}\frac{d\omega}{dp}$ ($\times 10^3$, in GPa^{-1}) determined from linear fits $\omega(p) = \omega_0 + \frac{d\omega}{dp}p$ to data points

	Zircon					HPLS				Reidite			
	ω^a_{exp}	ω^b_0	$d\omega/dp^b$	β^b_ω		ω^c_0	$d\omega/dp^c$	β^c_ω		ω^d_{exp}	ω^e_0	$d\omega/dp^e$	β^e_ω
E_g	202.5(1)	201.9(2)	− 0.60(4)	− 3.0(2)	E	115(5)	3.4(2)	30(3)	B_g	237.9(4)	240.7(5)	0.36(2)	1.4(1)
B_{1g}	214.9(1)	214.3(7)	1.33(7)	6.2(3)	B_1	221(4)	0.9(2)	4.0(9)	E_g	297.0(1)	297(1)	1.52(5)	5.1(2)
E_g	225.6(2)	225.1(3)	0.23(7)	1.0(3)	E	222(4)	0.3(2)	1.5(7)	A_g	326.4(1)	329.2(5)	0.65(2)	1.97(7)
E_g	357.4(1)	357.8(2)	4.26(4)	11.9(1)	E	451.1(7)	− 0.5(3)	− 1.2(7)	B_g	349(1)	364.8(9)	1.90(4)	5.2(1)
A_{1g}	440.0(1)	439.3(1)	1.42(5)	3.2(1)	A_1	454(2)	0.82(9)	1.8(2)	A_g	406.1(1)	406.2(7)	1.89(4)	4.7(1)
A_{1g}	975.6(1)	975.9(2)	4.92(4)	5.0(1)	A_1	1018(3)	2.7(2)	2.7(3)	B_g	465.8(2)	464.4(6)	1.91(1)	4.12(7)
B_{1g}	1009.0(1)	1009.4(3)	5.46(5)	5.4(1)	B_1	1044(5)	3.6(2)	3.5(2)	E_g	558.4(1)	558.2(5)	2.32(2)	4.15(5)
									B_g	610.9(7)	611.4(5)	1.96(2)	3.20(4)
									B_g	847.0(1)	848.5(9)	3.80(5)	4.47(6)
									E_g	886.4(1)	888.0(7)	4.21(4)	4.74(5)

The tabulated values are derived from the spectra of A2, which was also measured in $\bar{y}(xx)y$, where the zircon B_{1g} modes are much better pronounced; the values for A1 are the same within uncertainties;

[a] Experimentally measured at ambient pressure before compression;

[b] Determined from linear fits in the range 0–9 GPa;

[c] Determined from linear fits in the range 21–25.3 GPa;

[d] Experimentally measured at ambient pressure after decompression;

[e] Determined from linear fits in the range 10–21 GPa

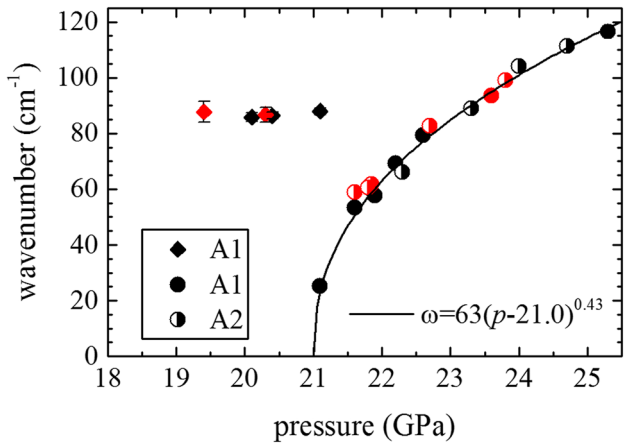

Fig. 3 Pressure dependence of the soft-mode wavenumber. Filled and semi-open symbols are data points collected from sample A1 and A2, respectively; circles represent the A_1 mode in the HPLS phase, diamonds the B_{1u} mode in zircon; red symbols correspond to data collected on decompression. The line is a power fit of type $\omega(p) = c(p - p_c)^n$, see the text for more explanations

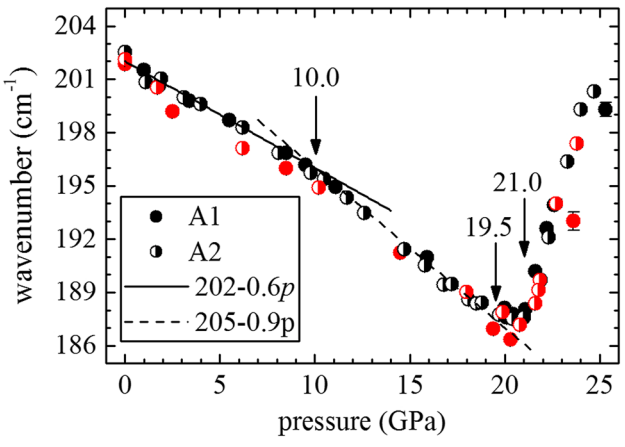

Fig. 4 Pressure dependence of the wavenumber of the phonon mode near 202 cm^{-1} (E_g in zircon, E in HPLS). Filled and semi-open symbols correspond to data for A1 and A2; red symbols are data collected on decompression. The solid and dashed lines are linear fits to the data points in the ranges 0–9 GPa and 11–17 GPa, respectively, collected on compression

peaks in this range, which at ambient pressure are positioned at ~ 357 and 440 cm^{-1} (see Table 2). The former peak arises from an E_g mode consisting of rigid SiO_4 rotations shearing the ZrO_8 polyhedra in (001), while the latter is generated by an A_{1g} mode comprising oxygen vibrations that flatten the SiO_4 tetrahedra along the *c*-axis, stretch the Zr–O bonds and twist the ZrO_8–ZrO_8 linkages (Stangarone et al. 2019a). At p_c, the zircon E_g and A_{1g} transform into E and A_1 phonon modes of the HPLS phase. The strong Raman intensity of these modes is indicative of large atomic vector displacements around the equilibrium atomic positions. The strongest Raman-active mode of reidite occurs at ~ 406 cm^{-1} at ambient pressure (see Fig. 2) and its wavenumber remains between the wavenumbers of the zircon/HPLS modes mentioned above in the entire pressure range (see Fig. 6). Similar to the zircon/HPLS peak near 440 cm^{-1}, this reidite phonon mode is fully

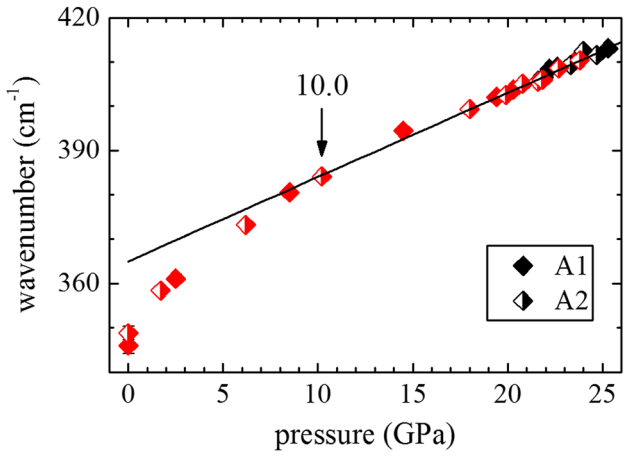

Fig. 5 Pressure dependence of the reidite phonon mode near 349 cm^{-1}. Filled and semi-open symbols correspond to data for A1 and A2; red symbols are data collected on decompression. The line is a linear fit to data points in the range 10–25.3 GPa (parameters given in Table 2)

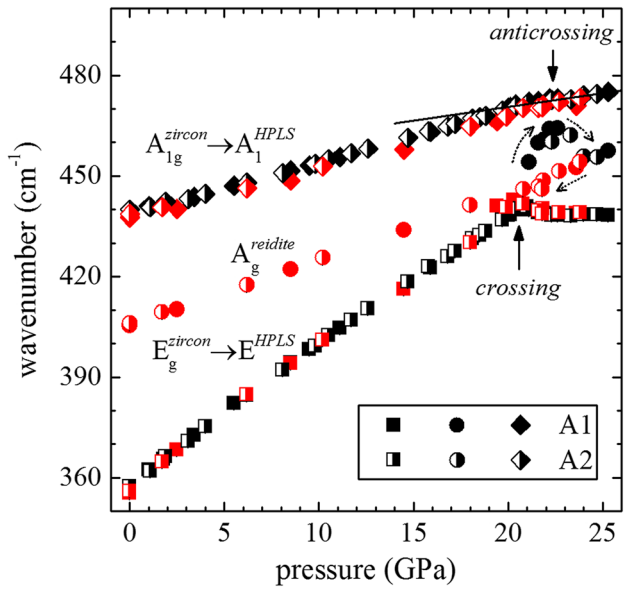

Fig. 6 Pressure dependence of the zircon phonon modes near 358 cm^{-1} (squares) and 440 cm^{-1} (diamonds) as well as of the reidite phonon mode 406 near cm^{-1} (circles). Filled and semi-open symbols correspond to data for A1 and A2; red symbols are data collected on decompression. The vertical arrows point to the phonon crossing and anticrossing points at ~ 20 GPa and 22.4 GPa, respectively. The dotted arrows mark the direction of pressure change in the data set for the A_g mode of reidite. The line is a linear fit to data points in the range 21–25.3 GPa (parameters given in Table 2)

symmetric (A_g in $I4_1/a$) and involves oxygen vibrations that flatten the SiO_4 tetrahedra and twist the edge-sharing ZrO_8-ZrO_8 linkages (Stangarone et al. 2019a). Simulated animations of the three phonon modes at zero pressure and temperature are included in the supplementary material. As can be seen in Fig. 6, on compression $\omega_{406}(p)$ exhibits a maximum near 22.4 GPa, where it is closest to $\omega_{440}(p)$, then it slightly decreases up to ~24 GPa and after that gradually increases. On decompression $\omega_{406}(p)$ linearly decreases with pressure and crosses $\omega_{357}(p)$ near 20 GPa, just below p_c. These results indicate ongoing transformation processes above 20 GPa and below 24 GPa with a maximum near 22.4 GPa. According to compatibility relations between irreducible representations (Dresselhaus et al. 2008) when two phonons of different symmetry are approaching one another in energy, they may be in resonance without losing symmetry (energy-level crossing), whereas if the phonons are of the same symmetry, they cannot truly cross each other but form an admixed state due to phonon–phonon interactions (energy-level anticrossing). Strictly speaking, the compatibility relations regard the dispersion of two eigenstates over the Brillouin zone (the reciprocal-space vector q is variable) at fixed thermodynamical parameters (e.g., p and T). However, the same approach can be applied to a system at a fixed q vector, in our case the Γ-point of the Brillouin zone, varying one thermodynamic parameter, namely, pressure p. Thus, based on the $\omega(p)$ relations at fixed T and q, we propose that reidite structural species start nucleating at the crossing point of $A_g(406)^{reidite}$ and $E_g(357)^{zircon}/E^{HPLS}$, but the switching to the reidite long-range order happens at the anticrossing point of $A_g(406)^{reidite}$ and $A_{1g}(440)^{zircon}/A_1^{HPLS}$, as a result of resonance admixture of two fully symmetrical phonon modes with a similar type of atomic vibrations. In general, the exact pressure at which phonon crossing and anticrossing occur should depend on the phonon compressibilities ($\beta_\omega = \frac{1}{\omega_0}\frac{d\omega}{dp}$) and expandibilities ($\alpha_\omega = \frac{1}{\omega_0}\frac{d\omega}{dT}$). Therefore, at relatively low temperatures, the formation of reidite long-range order is facilitated by the zircon-HPLS displacive phase transition occurring near the crossing point, and the reconstructive phase transition takes place just above p_c, whereas at elevated temperatures, the reconstructive phase transition to reidite may occur between p_r and p_c. Moreover, at high temperatures, the amplitudes of atomic vibrations are quite enhanced and an intermediate phase with SiO_4 tetrahedra already rotated about the zircon fourfold axis of symmetry is not necessary to facilitate the rebonding from a zircon to a reidite structure.

The HPLS phase seems to remain unaffected by the occurrence of reidite, because for all phonon modes $\omega(p)$ follows a linear trend in the range 21–25.3 GPa. Only above the pressure of the anticrossing point does the FWHM of the HPLS phonons increase due to stress applied by reidite–HPLS grain boundaries.

Phonon crossing to form incipient embryos followed by phonon anticrossing to switch the long-range order could be the driving force for reconstructive phase transitions in

general, but more experiments on other model systems are necessary to explore this problem.

The phonon compressibilties of the three $ZrSiO_4$ polymorphs for the observed Raman-active hard modes are compared in Table 2. It is worth noting that the phonon modes in zircon and HPLS phase are correlated by group–subgroup symmetry constraints because of the displacive character of the phase transition, whereas there should be no symmetry correlation with the reidite modes. Apart from $E_g^{zircon} \rightarrow E^{HPLS}$ near 202 cm^{-1}, which couples with the soft mode, the hard modes of the HPLS phase show smaller β_ω values than those for zircon and reidite. Therefore, at least dynamically, this phase is the stiffest $ZrSiO_4$ polymorph in the studied pressure range. The greatest change in β_ω at p_c is observed for $E_g(357)^{zircon} \rightarrow E^{HPLS}$, which cross in energy with the reidite A_g mode near 406 cm^{-1}. The compressibility of the $A_{1g}(440)^{zircon} \rightarrow A_1^{HPLS}$ phonon modes, which anticross with $A_g(406)^{reidite}$, reduces by approximately a factor of two at p_c. The SiO_4 stretching modes in the HPLS are also approximately twice more resistant to pressure than those in zircon (near 975 and 1009 cm^{-1}), whereas the corresponding modes in reidite, near 847 and 886 cm^{-1}, exhibit similar compressibilities to those in zircon.

Conclusions

The Raman spectroscopic analysis at room temperature in the pressure range up to 25.3 GPa experimentally proves the occurrence of a pressure-induced soft-mode-driven displacive phase transition at $p_c = 20.98(2)$ GPa from zircon ($I4_1/amd$) to a new HPLS phase ($I\bar{4}2d$). The space groups of the two phases form a group–subgroup relationship and hence the transition is allowed to be continuous, as observed. The change of the phonon compressibility of the zircon mode near 202 cm^{-1} and reidite mode near 349 cm^{-1} indicates that above $p_r = 10.0$ GPa zircon is in a metastable state with respect to reidite. These results experimentally validate the predictions of DFT calculations by Stangarone et al. (2019b).

At room temperature, the nucleation of regions with reidite intermediate-range order is facilitated by the presence of the HPLS phase as a structural bridge between zircon and reidite. The reconstructive change to reidite long-range order occurs ~ 22.4 GPa, as a result of energy anticrossing and admixture of two hard phonon modes from either phase, which are fully symmetric in the corresponding phase and consist of oxygen vibrations that flatten the SiO_4 tetrahedra along their $\bar{4}$ axes and twist the ZrO_8–ZrO_8 linkages. For arbitrary temperature, the pressure-induced reconstructive phase transition to reidite may occur at any pressure $p > p_r$, depending on how temperature shifts the pressures of phonon crossing and anticrossing, which in turn is controlled by the phonon compressibilities and expandabilities of the three $ZrSiO_4$ polymorphs.

Acknowledgements Financial support by the European Research Council (ERC grant 714936 to Matteo Alvaro, University of Pavia) and Deutsche Forschungsgesellschaft (MI 1127/7-2) is gratefully acknowledged. We thank Prof. Björn Winkler, Goethe-Universität Frankfurt, for the opportunity to use the He-gas loading setup available in his laboratory and Dr. Lkhamsuren Bayarjargal for help with gas loading.

References

Dresselhaus MS, Dresselhaus G, Jorio A (2008) Group theory: application to the physics of condensed matter. Springer-Verlag, Berlin

Klotz S, Chervin JC, Munsch P, Marchand GL (2009) Hydrostatic limits of 11 pressure transmitting media. J Phys D Appl Phys 42:075413

Knittle E, Williams Q (1993) High-pressure Raman spectroscopy of $ZrSiO_4$: observation of the zircon to scheelite transition at 300 k. Am Mineral 78:245–252

Kolesov B, Geiger C, Armbruster T (2001) The dynamic properties of zircon studied by single-crystal X-ray diffraction and Raman spectroscopy. Eur J Mineral 13:939–948

Kroumova E, Aroyo M, Mato JP, Kirov A, Capillas C, Ivantchev S, Wondratschek H (2003) Bilbao crystallographic server: useful databases and tools for phase-transition studies. Phase Transit 76:155–170

Momma K, Izumi F (2008) Vesta: a three-dimensional visualization system for electronic and structural analysis. J Appl Crystallogr 41:653–658

Montalvo S, Reddy S, Saxey D, Rickard WD, Fougerouse D, Quadir Z, Johnson TE (2019) Nanoscale constraints on the shock-induced transformation of zircon to reidite. Chem Geol 507:85–95

Munro R, Piermarini J, Block S, Holzapfel W (1985) Model line-shape analysis for the ruby R lines used for pressure measurements. J Appl Phys 57:165–169

Nasdala L, Smith D, Gaft RKM, Ziemann M (2004) Analytical perspectives in mineralogical research. In: Spectroscopic Methods in Mineralogy (A. Beran and E. Libowitzky, editors). EMU Notes in Mineralogy 6, Eotvos University Press, Budapest, pp 281–343

Ono S, Funakoshi K, Nakajima Y, Tange Y, Katsura T (2004) Phase transition of zircon at high P-T conditions. Contrib Mineral Pet 147:505–509

Pina Binvignat F, Malcherek T, Angel RJ, Paulmann C, Schlüter J, Mihailova B (2018) Radiation damaged zircon under high pressures. Phys Chem Minerals 45:981–993

Robinson K, Gibbs G, Ribbe P (1971) The structure of zircon: a comparison with garnet. Am Miner 65:782–789

Stangarone C, Angel R, Prencipe M, Camponenosi N, Mihailova B, Alvaro M (2019a) Measurements of strains in zircon inclusions by Raman spectroscopy. Eur J Mineral. https://doi.org/10.1127/ejm/2019/0031-2851

Stangarone C, Angel R, Prencipe M, Mihailova B, Alvaro M (2019b) New insights into the zircon-reidite phase transition. Am Mineral 104:830–837

van Westrenen W, Frank M, Hanchar J, Fei Q, Finch R, Zha C (2004) In situ determination of the compressibility of synthetic pure zircon ($ZrSiO_4$) and the onset of the zircon-reidite phase transition. Am Mineral 89:197–203